International Journal of Impact Engineering 105 (2017) 39–53

Contents lists available at ScienceDirect

International Journal of Impact Engineering

journal homepage: www.elsevier.com/locate/ijimpeng

Delamination properties of laminated glass windows subject to blast loading

Paolo Del Linz[a,b,*], Paul A. Hooper[b,*], Hari Arora[c,d], Yi Wang[b], David Smith[e], Bamber R.K. Blackman[b], John P. Dear[b,*]

[a] School of Civil and Environmental Engineering, Nanyang Technological University, Nanyang Avenue, 639798 Singapore
[b] Department of Mechanical Engineering, South Kensington Campus, Imperial College London, SW7 2AZ, UK
[c] The Royal British Legion funded Centre for Blast Injury Studies, Imperial College London, UK
[d] Department of Bioengineering, South Kensington Campus, Imperial College London, SW7 2AZ, UK
[e] Arup Resilience, Security and Risk, 13 Fitzroy Street, London W1T 4BQ, UK

ARTICLE INFO

Article History:
Available online 27 May 2016

Keywords:
Blast
Laminated glass
Delamination
Viscoelasticity
Numerical simulations

ABSTRACT

Delamination processes absorb significant amounts of energy in laminated glass windows when they are subjected to blast loads. Blast tests were performed previously and their results had been used to calculate the loads imposed on the support systems. In this research, the delamination process at realistic deformation rates was studied to understand the reaction force response obtained. Laboratory tensile tests were performed on pre-cracked laminated glass specimens to investigate their delamination behaviour. The experiments confirmed the presence of a plateau in the force-deflection graphs, suggesting that the delamination process absorbed significant energy. The experimental results were then employed to calibrate FEA models of the delamination process with the aim of estimating the delamination energy of the polyvinyl butyral (PVB) membrane and glass layers and its relationship with deformation speed. The delamination energies obtained through this research, if used with the appropriate PVB material model, are a valuable new tool new tool in the modelling and design of laminated glass façade structures.

1. Introduction

Blast threats represent an important design consideration for prominent building structures. Whilst all elements of buildings have to be designed considering their resilience to such threats, the façade, especially when composed of glass, requires special attention. A significant proportion of the injuries and economic losses are due to the failure of these components [1]. Façade failure can cause injuries to bystanders inside and outside the building both directly through fragments and indirectly through allowing blast pressures to penetrate the building envelope. Glass is a brittle material with relatively low fracture toughness and hence is not well suited to absorbing large quantities of energy. In a blast situation, it will fracture early, producing significant quantities of fragments [2]. Instead, laminated glass can absorb significantly a higher amount of energy by combining the strength of the glass layers with the ductility of an internal polyvinyl butyral (PVB) membrane bonded to the glass surfaces. When the shock wave reaches the laminated glass pane, the glass plies will tend to bend and the tensile stresses will cause them to fracture. However, the PVB layer can subsequently deform, absorbing energy whilst stopping the blast pressure from entering the building space and containing the glass fragments on its surface.

Whilst laminated glazing can offer much higher levels of protection than monolithic glass, the behaviour of all its components, including supports and connections, needs to be considered to assure the resilience of the structure. To estimate the design requirements for the components, it is important to understand the behaviour of the cracked laminated glass, as this will determine the loads imposed on other parts of the structure.

To improve this understanding, blast tests have been performed by several researchers, for example, Stephens [3], Zhang et al. [4,5], Kranzer et al. [6] and Larcher et al. [7]. Hooper et al. [8] performed tests using Digital Image Correlation (DIC) to collect full field deflection and strain data in 3 dimensions. The glass panes were composed of two 3 mm thick plies of annealed glass with a 1.52 mm PVB interlayer. The charges used were 12.8 kg and 25.6 kg C4 (15 kg and 30 kg TNT equivalent) and the stand-offs were between 10 and 16 m. These experimental data allowed the observation of the entire

* Corresponding authors. School of Civil and Environmental Engineering, Nanyang Technological University, Nanyang Avenue, 639798 Singapore. Tel.: 44 (0)20 7594 7086; Fax: +44 (0)20 7594 7017.
E-mail address: paolo@ntu.edu.sg (P. Del Linz), paul.hooper@imperial.ac.uk (P.A. Hooper), j.dear@imperial.ac.uk (J.P. Dear).

http://dx.doi.org/10.1016/j.ijimpeng.2016.05.015

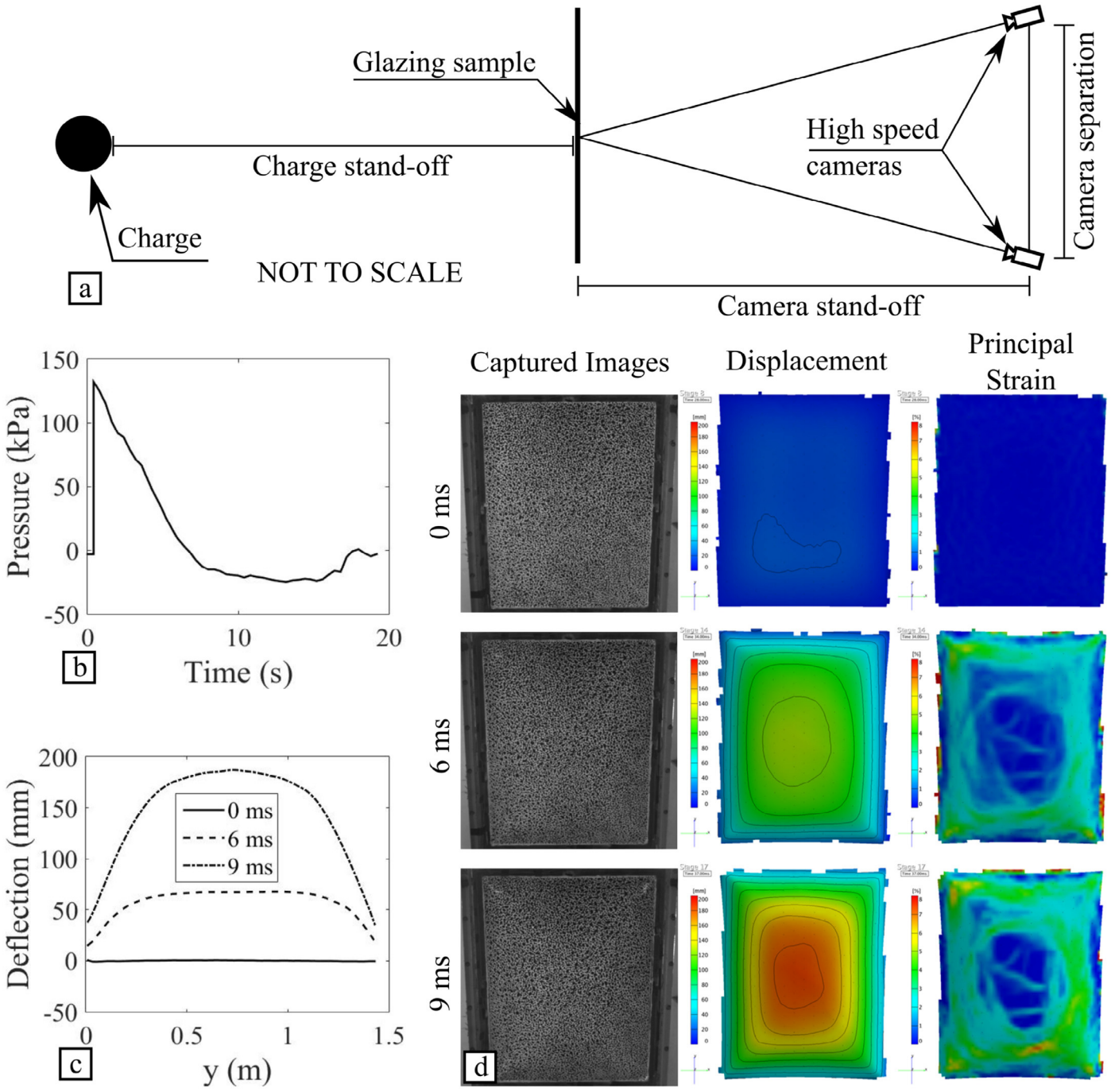

Fig. 1. Typical blast and DIC set up and results from a blast test (30 kg TNT equivalent at 16 m). The DIC set up is shown (not to scale) (a), together with the pressure time trace (b) and the deflected profile of the glazing sample (c). The raw high speed images and DIC results are also shown at the same three time points as the deflected profiles (d) (adapted from Reference 8).

loading process, starting from blast wave arrival, glass fracture and post-crack deformations. Typical graphical results are shown in Fig. 1 together with a diagram of the experimental set-up.

Additionally, Hooper et al. [8] placed several strain gauges around the window frame to estimate the reactions at discrete points around the frame. The results, whilst they included some noise, showed that the reactions at these discrete points did not increase significantly after an initial time.

These experimental data were employed by Del Linz et al. [9] to calculate the reaction forces along the entire perimeter. A typical result is shown in Fig. 2. It was noticed that the results strongly supported the presence of a plateau in the reaction forces at large deflections, as was first noticed in the early discrete reaction results.

The plateau in reaction force versus central displacement suggests that an energy absorption mechanism contributes in the absorption of the blast energy. Whilst the behaviour of the PVB membrane could account for this, a further possibility for such mechanism is progressive delamination of the glass fragments from the PVB membrane.

The performance of the glazing could be therefore dependent on the bond between the internal PVB membrane and the glass plies. These glazing panels are generally bonded in an autoclave, where

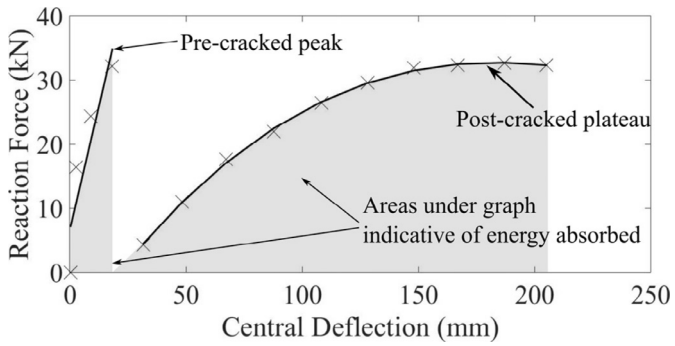

Fig. 2. Typical out of plane reaction force results for a blast test (adapted from Reference 9).

high pressures and temperatures can be applied to the glass and PVB layers. The bond in laminated glass is achieved through hydrogen links between the polyvinyl butyral molecule and the Silanol groups on the glass without the addition of specific adhesive compounds [10]. This bond is dependent on a number of factors related to the surface treatments applied to both substrates and the temperatures and pressures adopted during the bonding process [11,12]. Determining the properties of this interface would be important for the design of blast resistant windows, as well as the optimisation of the lamination design.

Researchers in the past have measured glass-PVB delamination energies at lower speeds. Rahul-Kumar et al. [13] performed compressive shear tests at different rates to obtain estimates of the cohesive strength of the bond. The results show the significance of strain rate for the delamination characteristics, with different peak stresses being reached during the different tests. Muralidhar et al. [14] performed tensile tests of laminated glass specimens with a central pre crack. A plateau could be seen in their force–displacement results. Delamination energies were then calculated assuming a hyperelastic material law for the PVB and subtracting its strain energy from the overall energy obtained from the force–displacement data. The same method was employed by Butchart and Overend [15], who considered two delamination speeds using a similar experimental set-up. In this case, the authors assumed a linear viscoelastic model to represent the PVB in their calculations. Whilst the results indicated a degree of rate dependency, further tests were deemed necessary to ensure these were not the results of uncertainties in the material models used. Iwasaki et al. [16] used samples bonded to PVB on just one side to perform similar tests. Speeds of up to 2.5 m/s were achieved, and a viscoelastic material law was assumed. In their results, similar energies were calculated for the speeds considered. Recently, Pelfrene et al. [17] performed peel tests with different types of PVB interlayers. Pelfrene et al. performed the tests at 127 mm/min peeling speed and measured the energies using a finite element analysis (FEA) model of the system. All these studies found delamination energies ranging from 20 to 1000 J/m^2.

The deformation rates during a blast will be significantly faster than those seen in these experiments. In this research, laboratory experiments were performed at speeds ranging from 0.01 m/s to 10 m/s. FEA was then used to simulate the delamination process. High strain rate PVB tensile test results were used to fit a hyperelastic viscoelastic material law and cohesive zone modelling was used to represent the delamination of the two components. Using a more complex material model will improve the estimates of the strain energy absorbed by the material, which will in turn allow for more precise estimate of the adhesion energies, especially at higher deformation speeds. The models were then used to fit the delamination energies at the different deformation speeds and to compare the system behaviour to that observed during the experiments.

2. Method

2.1. Experimental

The samples used for the delamination experiments employed Saflex PVB with thicknesses of 0.38 mm, 0.76 mm, 1.52 mm and 2.28 mm. The thickest layer was prepared by bonding 1.52 mm and 0.76 mm layers. To do this, the two layers of PVB were placed on top of each other between the glass sheets in the autoclave when preparing the laminated glazing samples, using the same pressure and heating combination to ensure their adhesion. Except for the thickness, the material formulations were identical for all the products. No special procedure was adopted when preparing the laminated glazing samples, which were bonded using standard autoclave treatments by a commercial company.

The specimen dimensions were 150 mm × 60 mm with 3 mm thick glass plies and were cut from a glass sheet using a water jet cutter. Aluminium end tabs 2 mm thick were bonded to the samples to connect them to the testing machine. These 2 mm tabs were bonded using a toughened methacrylate adhesive (Araldite 2021 manufactured by Huntsman Advanced Materials). The glass on both sides of the samples was then cut in the centre of its length in corresponding positions on each side. This was achieved by scoring the glass and then propagating a crack by tapping with a ball hammer. The samples are shown in Fig. 3.

The experiments were performed on a servohydraulic Instron VHS high strain-rate test machine capable of 25 m/s deformation speed with a 20 kN maximum load. As the instrument was

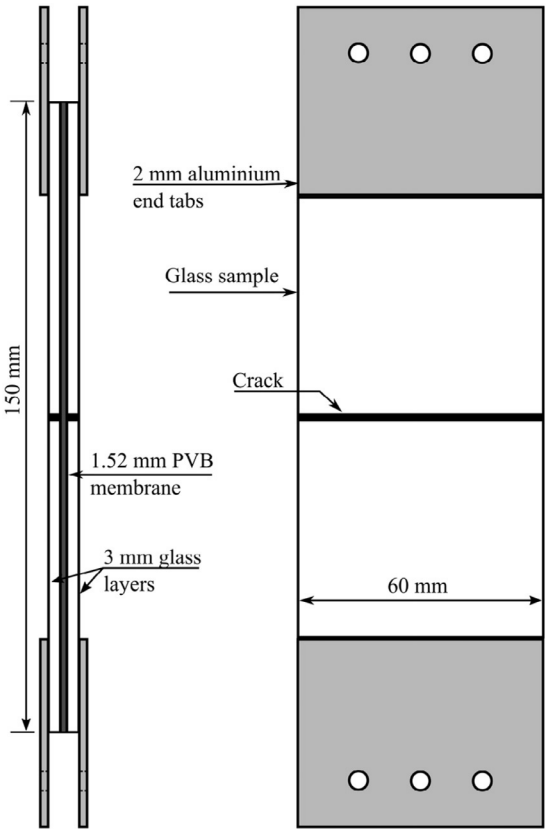

Fig. 3. Geometry of the 1.52 mm PVB thickness experimental samples used. The samples using other interlayer thicknesses were similar.

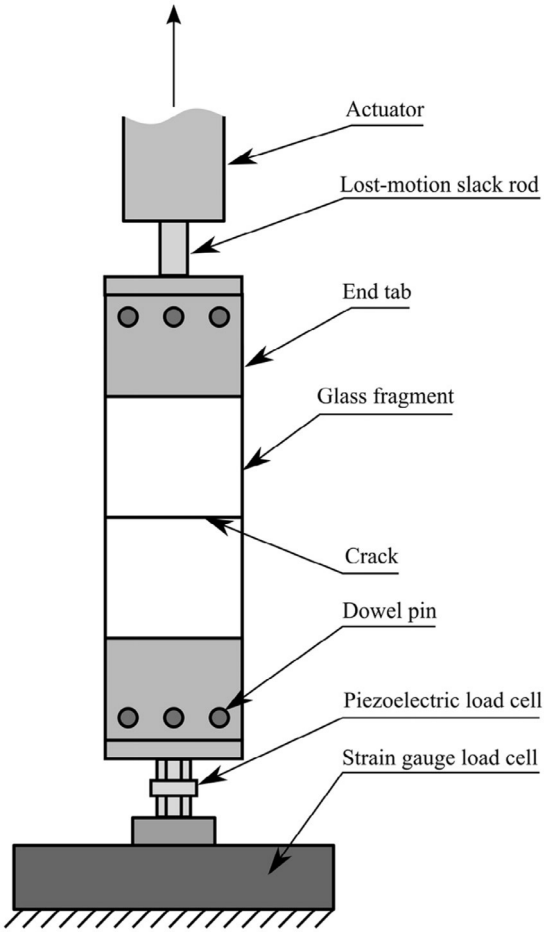

Fig. 4. Experimental set up for the delamination tests [17].

customised for installation in the laboratory, it was not part of a standard manufacturer model series. All components of the set up were kept to the lowest mass possible to minimise transient forces during the initial acceleration phase. Additionally, to ensure the sample would be loaded at a constant speed, a loss-motion device was placed between the actuator arm and the sample. This ensured that the specimens would be displaced only after the machine reached its programmed speed. For speeds above 0.1 m/s, a piezoelectric load-cell (Model 222B manufactured by PCB Piezotronics Inc.) was employed to measure the applied loads. A strain gauge load cell was used at lower speeds. Fig. 4 shows a diagram of the experimental set up whilst Table 1 presents a list of the experiments performed, including the sample dimensions, interlayer thickness and deformation speed.

Polarizing filters and high speed photography were used to record the delamination progression and general deformation of the samples. PVB and glass are birefringent materials under stress; therefore, a clear boundary was visible between delaminated and bonded areas as the stress levels in the PVB membrane change sharply at this location. This information was used to calculate the overall strain in the PVB ligament as well as to track the speed of the delamination, which was compared to that in FEA analysis results. This delamination process is shown in Fig. 5. An automatic procedure was prepared using MATLAB to locate areas where the gradient of the intensity of the colour was highest. These areas indicated the location of either a delamination front or of a glass edge and recorded its position. The distance between the uppermost two locations and the lower two was then calculated, thus providing the length of the delaminated area in the picture. The procedure was

Table 1
Tests performed on cracked laminated glazing samples.

Specimen dimension (mm)	Interlayer thickness (mm)	Pulling speed (m/s)
150 × 60	0.38	0.01
150 × 60	0.76	0.01
150 × 60	1.52	0.01
150 × 60	2.28	0.01
150 × 60	0.38	0.1
150 × 60	0.76	0.1
150 × 60	1.52	0.1
150 × 60	2.28	0.1
150 × 60	0.38	1
150 × 60	0.76	1
150 × 60	1.52	1
150 × 60	2.28	1
150 × 60	0.38	10
150 × 60	0.76	10
150 × 60	1.52	10
150 × 60	2.28	10

repeated on all images and the speed of delamination was obtained. Selected images were analysed manually to validate the automated procedure.

The forces recorded during the experiment were analysed to measure the plateau level which developed in the tests. After an initial peak due to inertial forces during the sample acceleration, the plateau level was reached. This was measured through the mean of the data between $t = t_s + 0.4(t_e - t_s)$ and $t = t_s + 0.8(t_e - t_s)$, where t was the test time, t_s was the start time of the test and t_e was the end time of the test. These points were chosen so that transient forces, due to the initial acceleration and the final sample failure, were excluded from the calculation. The engineering stresses in the PVB were also calculated from the force data. The true stresses were not found as the strain level in the interlayer varied along the ligament, increasing when further away from the delamination fronts, rendering an overall estimate only indicative.

2.2. Delamination energy analysis

The procedure to calculate the delamination energy from these tensile tests involves subtracting the strain energies of the system from the total energy found from the force–displacement trace. Whilst the strain energies could include components from both the PVB and the glass, the PVB contribution will generally be

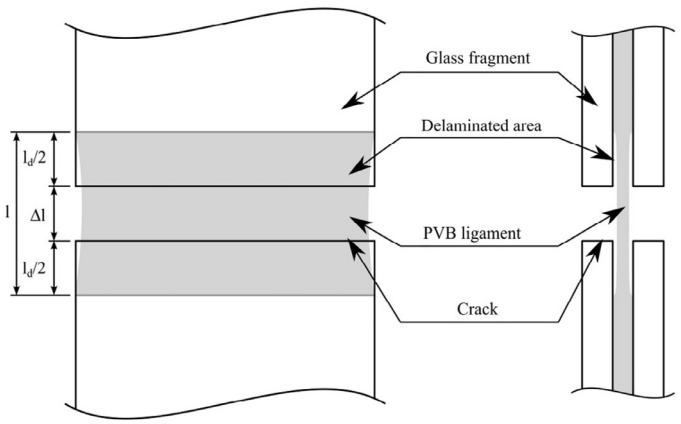

Fig. 5. Diagram showing the delamination process around the crack of the glass layers.

significantly larger, due to the greater strain levels. In previous work [14–16], the glass contribution was ignored, and PVB material models for which a close form solution of the equations exist have been used to calculate strain energies.

In the present work a material model including both non-linear hyperelasticity and viscoelastic effects has been formulated. A closed form analytical solution for the delamination energy does not exist with this material model and a finite element model employing cohesive elements was used to account for strain energies.

2.2.1. PVB material model

Several authors conducted experiments on the PVB material to determine its properties. Vallabhan [18] obtained shear modulus estimates from tests on laminated glazing, whilst Du Bois and Timmel [19,20] used experimental data to include hyperelastic representations of the material in their work. The rate dependency of the material has been considered also by Xu and Li [21], who used viscoelastic formulations in their models. The same authors also performed high strain rate tests on the material to improve their material model [22]. Iwasaki and Sato noticed a change in behaviour in the PVB at higher rates [23], noting that the initial stiffness of the material raised sharply at higher deformation speeds. The same authors also produced a viscoelastic material model for the lower rates [16]. The shift in behaviour was again noticed by Morrison [24], Hooper et al. [25], Liu and Sun [26] and Zhang et al. [27]. Hooper et al.'s [25] tests were conducted on servohydraulic machines and a range of strain rates was covered, from $0.2\,s^{-1}$ to $400\,s^{-1}$. These results, complemented with results at lower rates of $0.01\,s^{-1}$ to $0.2\,s^{-1}$, were employed in this work to produce a material model which could be used in finite element modelling. As mentioned above, in the experiments the PVB material showed high strain rate sensitivity. At low strain rate the material deforms as a rubbery hyperelastic material. However, when deformed at high strain rate it presents an initial stiff, almost linearly elastic phase, followed by a non-linear deformation.

A two term reduced polynomial strain potential was used for the hyperelastic part of the material model, as shown in Equation 1:

$$W = C_1 * (I_1 - 3) + C_2 * (I_1 - 3)^2 \tag{1}$$

where W is the strain energy density, $I_1 = \lambda^2 + 2\lambda^{-1}$, λ is the stretch $(1+\varepsilon)$, and C_1 and C_2 are material constants representing the stiffness of the material.

A Prony series was included to represent the viscoelastic aspects of the material behaviour. The expression for this model for a step relaxation test is:

$$\sigma = \sigma_0\ (\varepsilon) * g(t) \tag{2}$$

with

$$g(t) = g_\infty + \sum_1^N g_i \exp\left(-\frac{t}{\tau_i}\right) \tag{3}$$

where σ is the actual stress in the material, $\sigma_0(\varepsilon)$ is the instantaneous hyperelastic stress, $g(t)$ is the viscous component given by the Prony series, and g_i, g_∞ and τ_i are the Prony series parameters. In total, six critical times ranging from 1.0×10^{-6} s to 1000 s were considered, though the fitting procedure produced a constant of 0 for the highest critical time, effectively reducing the series to five terms. The method described by Goh et al. [28] was employed to calibrate the material model using the experimental data. A square minimization technique was applied to determine the coefficients. The coefficients obtained are listed in Tables 2 and 3. The experimental results with the model fit are shown in Fig. 6 for the slowest, fastest and an intermediate test speeds.

Table 2
Hyperelastic material model parameters used for the PVB.

Parameter	Overall fit value	Low rate fit value
C1 (MPa)	311	92.6
C2 (MPa)	20.6	56.1

Table 3
Prony series models parameters used for the PVB.

τ_i (s)	Overall fit g_i	Low rate fit g_i
1×10^{-6}	5.04×10^{-05}	0.0147
1×10^{-5}	0.9626	0.959
1×10^{-3}	0.00652	1.18×10^{-5}
0.1	0.007946	0.00237
10	0.0135	0.0145
1000	0	0.00886

To consider the effect of the material model on the delamination behaviour, an additional material model was employed. For this, the fit was performed with curves below and including $0.2\,s^{-1}$, producing a much more compliant model which approximated more closely the low rate behaviour. This fit is shown in Fig. 7 and its constants are listed in Tables 2 and 3.

2.2.2. FEA modelling

ABAQUS release 6.10 [29] was used for the delamination energy analysis. The models included three main components, the PVB membrane, the glass layers and a cohesive layer on each side of the PVB connecting it to the glass. A half model with a vertical symmetry condition was used to increase the computational efficiency. A 5 mm high damping element was introduced to reduce transient vibrations in the model.

The model overall dimensions were 150 mm × 30 mm. The glass layers were 3 mm thick and 140 mm high overall. They were split in two sections, above and below the crack, each 70 mm in length. A PVB thickness of 1.52 mm was chosen as it is the most relevant for blast loading designs. The cohesive zone was modelled with 0.01 mm thick element layers on each face of the PVB. These were tied to the glass faces. Fig. 8 shows the geometry of the models with the main dimensions.

The glass plies were meshed with 1 mm cubic stress elements (C4S4). The same elements were used for the PVB, reducing their thickness to 0.76 mm so that there were two elements in the thickness direction. A mesh sensitivity analysis was run for the faster, 10 m/s, models. Models were run with a 0.5 mm mesh and the results showed differences with the 1 mm mesh models of less than 5% in the initial stresses. The stability of the models was however significantly decreased, which increased computer times and precluded obtaining plateau stresses results. It was therefore decided that the 1 mm mesh would be used for subsequent models.

The material models used are summarised in Table 4. Glass was represented using linear elastic material properties and the PVB was modelled with the reduced polynomial viscoelastic models described above. The cohesive element model used is described below.

2.2.3. Cohesive modelling

Cohesive zone modelling (CZM) was used to represent the delamination. The peak stress, initial stiffness and a degradation law need to be defined to fully represent the adhesion layer, as described by Chandra et al. [30]. It was decided to use a bilinear formulation, therefore assuming a linear behaviour for the post peak decay. The stress displacement behaviour of this formulation and the key

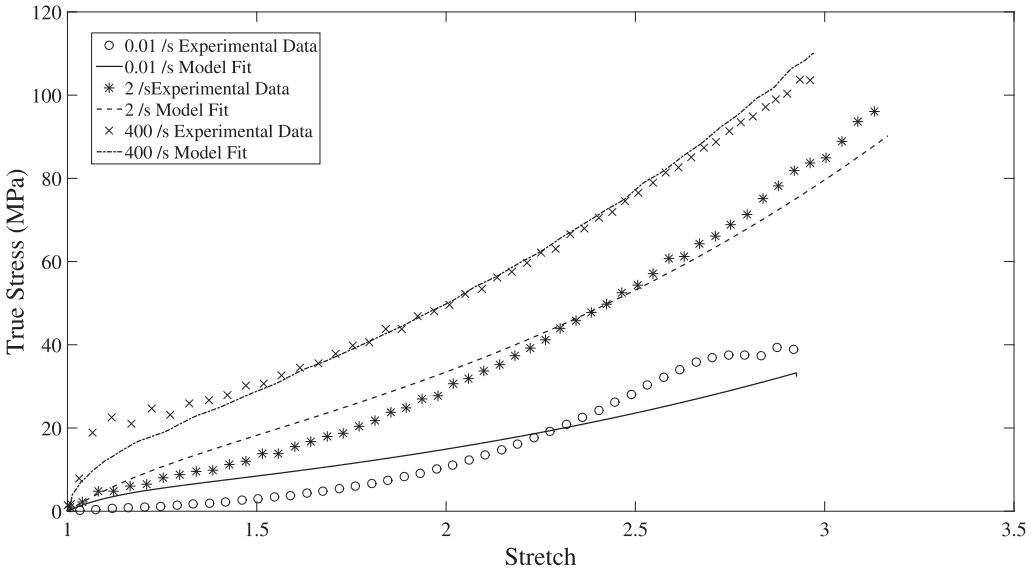

Fig. 6. Material model fit for the PVB.

parameters defining the model are shown in Fig. 9. Whilst the failure was likely to be a combination of mode I and mode II mechanisms, it was challenging to separate these effects in the tests. Muralidhar et al. [14] explained that for this situation, mode-mixity can be ignored. In these models the same parameters were therefore included for all modes. A quadratic damage initiation model defined in Equation 4 was used [29].

$$\left\{\frac{S_n}{S_n^o}\right\}^2+\left\{\frac{S_s}{S_s^o}\right\}^2+\left\{\frac{S_t}{S_t^o}\right\}^2 \tag{4}$$

where S_n, S_s and S_t are the stresses in the normal and the two shear directions and S_n^o, S_s^o and S_t^o are the capacities for the same modes.

Traction elasticity had to be used in the pre-peak phase. It was assumed that the cohesive material would be similar to the PVB bulk material. A mesh size of 1 mm square and of 0.01 mm thickness was assumed and the Young's modulus derived by Hooper [31] was used to calculate the stiffness parameter (k). A Poisson's ratio of 0.5 and isotropic behaviour were then assumed to calculate a shear modulus. Whilst such a Poisson's ratio could have caused numerical instabilities if employed directly in the model, it was not used in such manner in the material formulation used and the traction separation models proved stable without any noticeable issue. To check the sensitivity of the results to this calculated stiffness, the model was also run with stiffness of 1 MN/m and 1 GN/m. No significant changes were seen in the results. This agrees with the observations of Pelfrene et al. [17], who also noticed the debonding behaviour to be relatively insensitive to the cohesive zone model exact shape.

The peak stress (S) was found using data from Rahul-Kumar et al. [13], where the debonding behaviour was studied in shear tests at different strain rates. The peak stresses at different rates were plotted and a logarithmic law was fitted to these, as shown in Fig. 10. The fit to the data is given by:

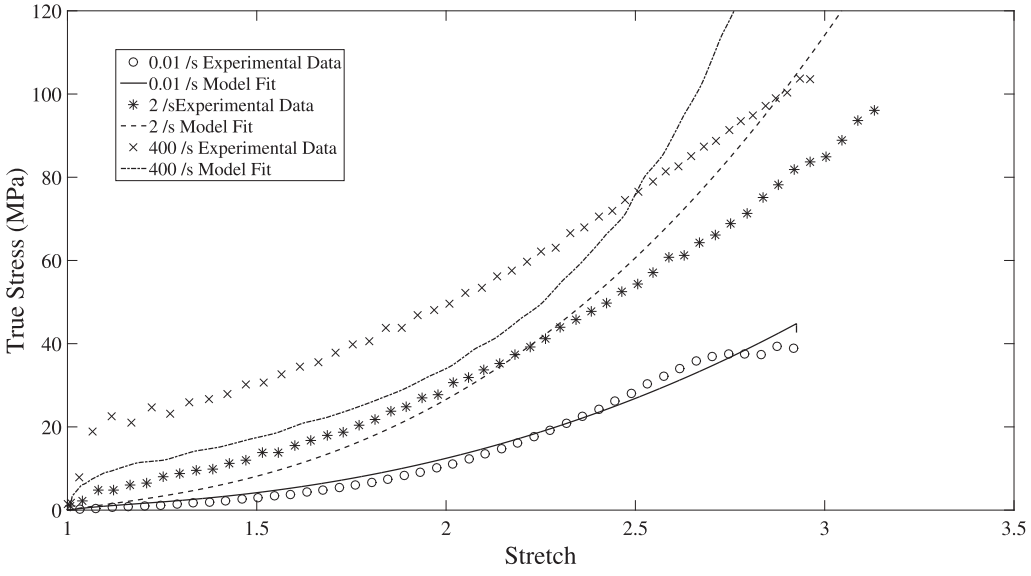

Fig. 7. Low strain rate PVB model fit.

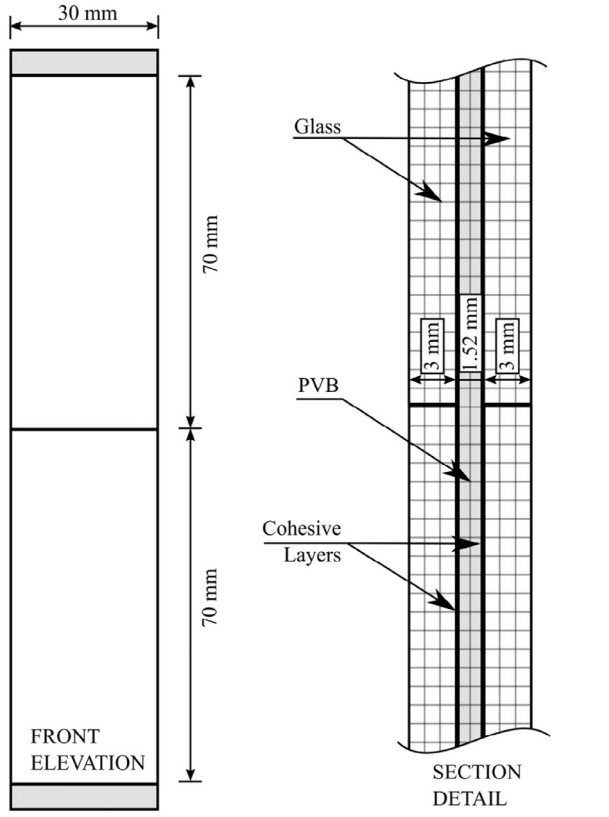

Fig. 8. Main dimensions and features of the single crack delamination models. The section detail also shows the mesh used.

$$S = 0.782 \ln(\dot{\varepsilon}) + 8.22 \quad (5)$$

where S is the peak stress and $\dot{\varepsilon}$ is the strain rate. Table 5 shows the peak stresses used in the models.

2.2.4. Data analysis

The models described above were run for the 0.01, 0.1, 1 and 10 m/s tests. The main objective was to measure the delamination energies for each of these deformation speeds, as this parameter would be most useful for further analysis of the system. All the models were run for a minimum 30 mm displacement to ensure the stress plateau would be firmly established. The key results to be extracted from the models were the plateau stresses and the delamination speeds. The plateau stresses needed to be matched to the experimental data as they were used as the indication of the quality of the cohesive model fit. This was achieved by modifying the cohesive model's ultimate displacement. The CZM input could then be used to calculate the energies of delamination, which was compared between the different deformation speeds. The delamination speed was also extracted for comparison with experimental results. Element failure data at different time steps were used for this.

Table 4
Summary of the material models employed in FEA models.

Material	Model type	Summary of parameters
Glass	Linear elastic	$E = 70$ GPa, $\rho = 2500$ kg/m^3, $\upsilon = 0.22$
PVB	Viscoelastic – Prony series with a reduced polynomial spring	See Table 2 for fit parameters
Cohesive elements	Traction separation	$k = 53$ MN/m

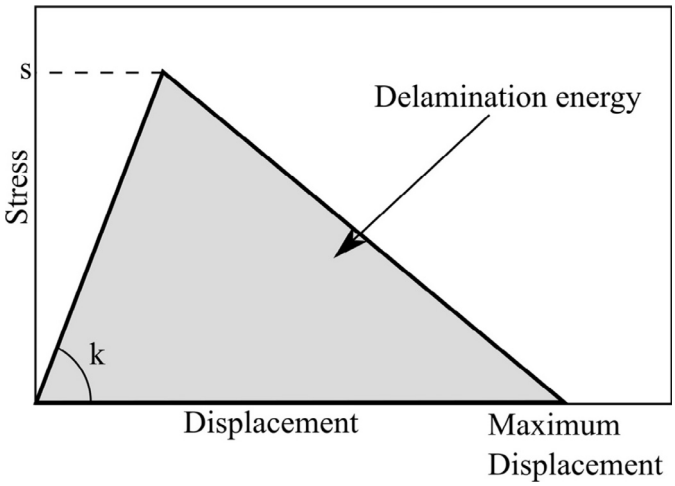

Fig. 9. CZM stress displacement formulation assumed for the FEA model. The delamination energy is the area underneath the assumed curve.

3. Results

3.1. Experimental

Fig. 11 shows the delamination progression during a test. The deformation speed was 1 m/s in this case. The ligament stretched, whilst the delamination front propagated further into the glass, as seen in the second frame. Finally, the PVB tore in the last frame. The force per unit width versus extension and strain versus extension are shown in Figs. 12–15 for all the test speeds. The force was seen to increase sharply, reaching a transient peak partly due to inertial forces, before decreasing to a plateau level as expected. Thicker interlayers showed a lower ligament strain than the thinner interlayers. As a certain force level is required to start the delamination process, this will cause higher stresses, and hence strains, in thinner interlayers. The variation in gradients in the strain information also suggests a change in the overall strain rate in the PVB. At a speed of 0.1 m/s, the initial rate was calculated to be between 25 s^{-1} and 11 s^{-1} depending on the interlayer thickness. These rates then reduce to 0.6 s^{-1} at a later stage in the test. In general, higher initial strain rates were seen for all cases. For example, the 10 m/s tests showed initial rates in the order of 4000 s^{-1}. The failure mode for the 0.01 m/s tests was the complete delamination of the glass from the PVB. Instead, at all higher speeds the failure condition switched to PVB tearing. Lower extensions were measured for the two thinner interlayers. For example, at 0.1 m/s deformation speed, the 0.38 mm interlayer failed at an extension of 8 mm and the 0.76 mm failed at an extension of 24 mm. The two thicker interlayers failed by tearing gradually at extensions above 30 mm. This is connected to the higher strains seen in the lower thickness interlayers mentioned above. In the 0.38 mm thickness case, the strain rose rapidly to 150% before failure. Instead, in the thicker interlayers the ligament strain remained lower, increasing the failure time. Failure happened eventually at strains close to 100%. Similar behaviours were seen in the higher speed tests. However, as additional glass cracks obscured the details of the PVB behaviour, strains in thickest, 2.28 mm, interlayers were not measured beyond 10 mm deformation, preventing an estimate of the plateau behaviour. Additionally, large oscillations were present in the force measurements at 10 m/s due to the momentum of the sample grips and load-cell. Table 6 summarises the maximum force F_{max}, maximum

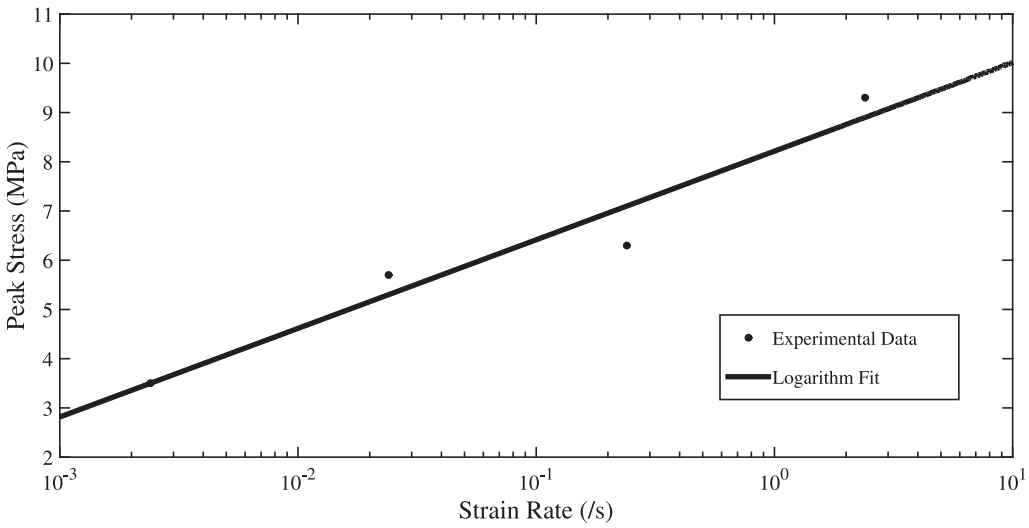

Fig. 10. Peak stress against the strain rate from Rahul-Kumar et al. [13].

Table 5
Peak stresses used in the models.

Speed (m/s)	Peak stress (MPa)
0.01	5.88
0.1	7.68
1	9.48
10	11.28

PVB engineering stress σ_{max}, plateau force F_p and plateau PVB engineering stress σ_p for each sample tested. It shows that although the force per unit width increases with increasing interlayer thickness, the stress in the ligament decreases.

The experimental images were also used to calculate the delamination speeds. Fig. 16 shows a sample image with the identified location of the delamination fronts and glass edges. These were always measured away from the curved edges, in the flat central area, as indicated by the vertical line in the image. The measurement though was not taken necessarily in the centre of the samples, as cracks developing in the glass in some cases obscured the view in that specific location earlier than elsewhere. In general, a location where data could be extracted for as long as possible was selected. The results showed that the speed of delamination varied to a small degree during the experiment. However, as the uncertainties were larger than these variations, it was considered appropriate to use a constant velocity for further stages of the analysis. An error of ±1 pixel per line was assumed. As four such locations had to be determined, the worst case total error was found to be ±4 pixels. Considering this and the total delaminated distance to be measured, the overall error was estimated to be 5%. The data obtained are shown in Table 7 together with the estimated errors.

3.2. FEA modelling

Fig. 17 shows the results for all speeds. The models show an initial steep rise in the stresses followed by a plateau area. This is similar to what was observed in the experiments. The main difference is that the initial oscillations seen in the experimental data at higher speeds are not observed in the FEA results due to the damping elements.

Fig. 18 shows the stress distribution at different times during the deformation. It can be seen that, similarly to the experimental images, the delamination begins at each glass edge, and extends progressively towards the middle of the glass fragments. The image also shows that the delamination front shows a slight curvature near the edge of the glass. This is similar to what was seen in experimental images such as those shown in Fig. 11.

The delamination front is shown in detail in Fig. 19. In this side view of the model, it can be seen that the stress level in the PVB not yet delaminated is close to 0, as the stiffness of the glass is significantly higher. The stresses increase very rapidly near the delamination front. The delaminated PVB layer also reduces significantly its thickness, as the tensile stresses are sizeable. This might largely reduce the friction between the glass and the polymer in these types of tests. Table 8 shows the results from the analysis for the various speeds. The energy was determined by the CZM parameters which were used for the simulations which matched the plateau PVB engineering stresses recorded in the experiments. There was a large variation in the delamination energy with the deformation speed. At 0.01 m/s, the energy was 90 J/m^2, whilst it reached 3000 J/m^2 at 1 m/s, with delamination speeds ranging from 0.083 m/s to 15.67 m/s. The 10 m/s case was also fitted using the low rate PVB material model, giving an energy of 9000 J/m^2 and a delamination speed of 10.8 m/s.

The variation in delamination energies seems to reduce at higher speeds, implying that this parameter is less sensitive to velocity increases after a speed around 1 m/s is reached. It should be noted that the delamination speed differs slightly from the measured value. This difference was greater for the lower deformation speed and reached a minimum for the 1 m/s case.

4. Discussion

The experiments performed allowed the measurement of the delamination plateau forces experienced by the samples. The measurements of these data were taken once the stable plateau level of the forces had been established. Whilst at lower speeds this was easily determined, in the 10 m/s case the initial vibrations had not fully stopped in the available data, as can be seen in Fig. 15. Zhang et al. [32] remarked that for tests to produce acceptable results, at least 3 cycles of vibrations were required to go through the sample. If this is calculated using the wave speed in glass for approximately 140 mm and PVB for 10 mm, allowing therefore for the delamination to have already progressed, the vibration time is equal to:

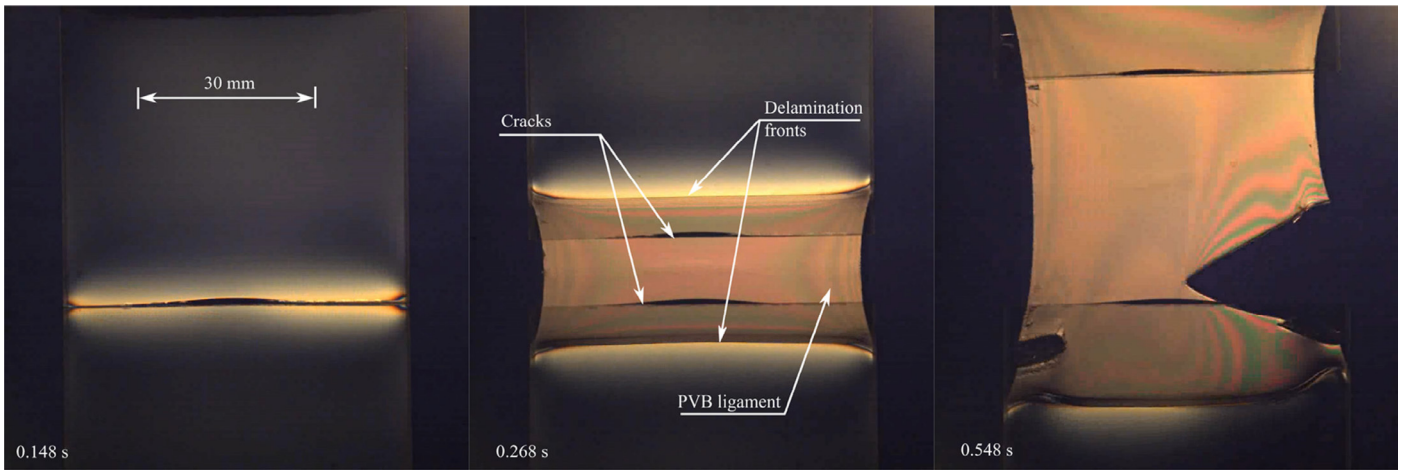

Fig. 11. Experimental images of the delamination tests showing the process delamination.

$$V_g = \sqrt{\frac{70 \times 10^9}{2500}} = 5290\,\text{m/s}$$

$$V_p = \sqrt{\frac{1 \times 10^9}{1100}} = 953\,\text{m/s}$$

$$t_w = \frac{2 \times 0.14}{5290} + \frac{2 \times 0.01}{953} = 7.39 \times 10^{-5}\,\text{s}$$

where V_g and V_p are the wave speeds in the glass and PVB, respectively, and t_w is the time required for a full cycle. At the fastest testing speed, the test lasted for more than 20 mm before the sample failed. This would give a testing time of above 2 ms, one order of magnitude larger than the ringing frequency, ensuring that a uniform stress state could be reached in the sample. Additionally, the testing system was similar to that used by Hooper et al. when testing PVB [25]. In that occasion, the authors checked the system vibration frequency through a sudden load removal. The period measured was 2.9×10^{-4} s, again one order of magnitude below the length of the test.

Whilst the sample vibrations were still noticeable throughout the test, their intensity reduced significantly and, after the first few peaks, the stresses oscillated about a mean value corresponding to the assumed plateau stress, as can be seen in Fig. 15. The images used for the delamination extent measurements could also be used to calculate the speed of the top section of glass. This is shown in Fig. 20, which shows that within the first 5 to 10 mm of displacement, the sample reached and surpassed the target speed. Subsequently, the speed oscillates about the value of 10 m/s. The graph stops at 20 mm as, though the PVB had not failed yet, the glass edge had cracked and measuring its speed proved impossible after this point. This is the same reason for which a similar limit is adopted in the results shown in Fig. 15. Both these observations supported the assumption that the initial inertial forces would have dissipated by the time the plateau stress was measured. Nevertheless, significant oscillation about the mean values of the speed and force measurements could be seen throughout the data collected. It is likely that this did reduce the accuracy of the plateau force estimate, possibly explaining the small drop in energy observed between this speed and 1 m/s. However, the energy estimates were the product of several modelling assumptions, including the PVB material model, which was shown to have a potentially very large effect on the energies measured. Therefore,

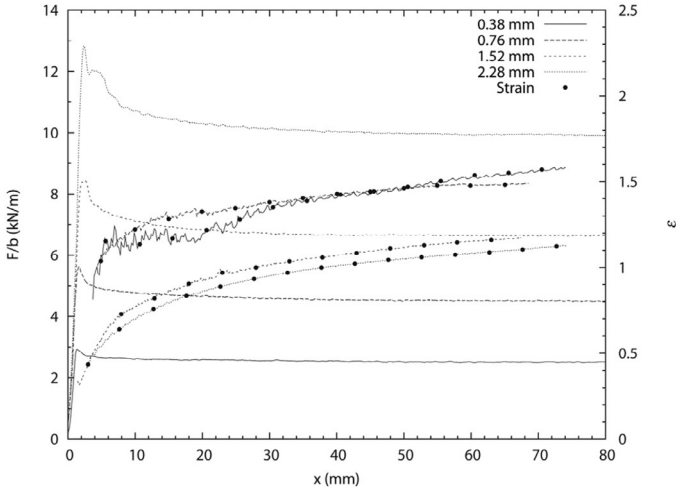

Fig. 12. Experimental force per unit width and strain against the overall deformation for the 0.01 m/s experiments.

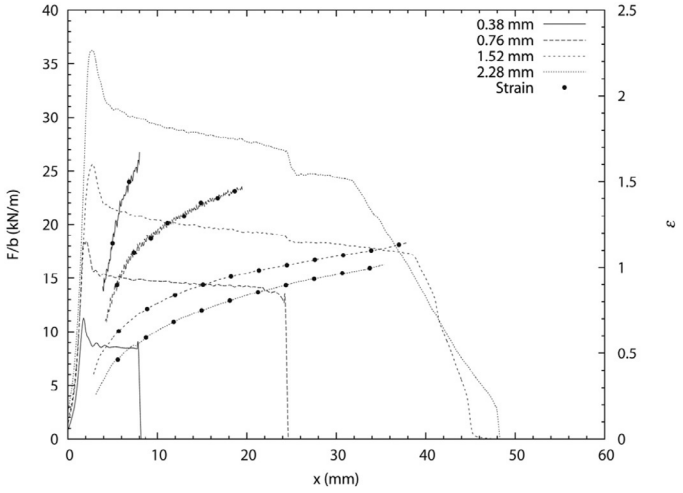

Fig. 13. Experimental force per unit width and strain against the overall deformation for the 0.1 m/s experiments.

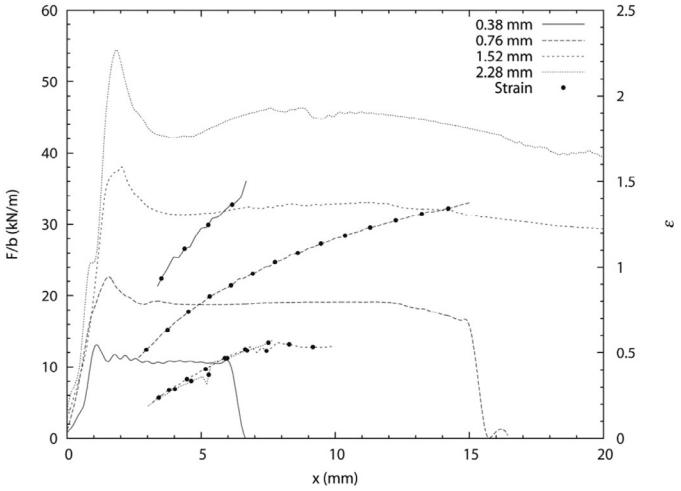

Fig. 14. Experimental force per unit width and strain against the overall deformation for the 1 m/s experiments.

Table 6
Experimental results of delamination tests. Peak and plateau forces and stresses are listed.

Test speed (m/s)	Interlayer thickness (mm)	F_{max} (kN/m)	σ_{max} (MPa)	F_p (kN/m)	σ_p (MPa)
0.01	0.38	3	7.9	2.5	6.6
0.01	0.76	5.6	7.4	4.5	5.9
0.01	1.52	8.4	5.5	6.6	4.3
0.01	2.28	12.8	5.6	10	4.4
0.1	0.38	11.1	29.2	8.7	22.9
0.1	0.76	18.3	24.1	14.7	19.3
0.1	1.52	25.6	16.8	20	13.2
0.1	2.28	36.2	15.9	28.8	12.6
1	0.38	13.3	35	10.8	28.4
1	0.76	22.6	29.7	19.2	25.3
1	1.52	38	25	32.3	21.3
1	2.28	54.4	23.9	44.8	19.6
10	0.38	49	129	–[a]	–[a]
10	0.76	74	97.4	24	31.6
10	1.52	117	77	40	26.3
10	2.28	–[b]	–[b]	–[b]	–[b]

[a] No plateau was observed in the data.
[b] The glass failure was too extensive before the delamination was observable.

it is unlikely that the imprecisions in this force measurement will lead to more significant uncertainties.

The experimental stress measurements and FEA techniques used allowed the estimate of the delamination energies connected to several deformation speeds of the samples. As shown in Table 8, the results rise between the slower test, 0.01 m/s and 1 m/s. The energy is then more stable between this speed and 10 m/s, though previously mentioned experimental uncertainties could have affected the details of this result. The results were plotted in Fig. 21 against the overall deformation rate, calculated using the deformation speed and the sample size.

The results showed significantly higher delamination energies than those seen in previous studies for all cases except for the 0.01 m/s speed. However, the speeds used for these experiments were significantly higher than those of other works. For example, the peel speed used by Pelfrene et al. [17] was 127 mm/min. The delamination speed for the 0.1 m/s deformation tests was 79 mm/s, or 4740 mm/min, 37 times higher than Pelfrene et al.'s. Whilst research on the causes of such rate dependency is ongoing, several authors have in the past attempted to explain these differences using viscoelastic models, which could also explain the differences seen here [33]. Such rate sensitive delamination models have been implemented in some software [34]; however, they can be difficult to use. For example, even in the case studied here, it would be challenging to separate the overall strain rate of the PVB material to that

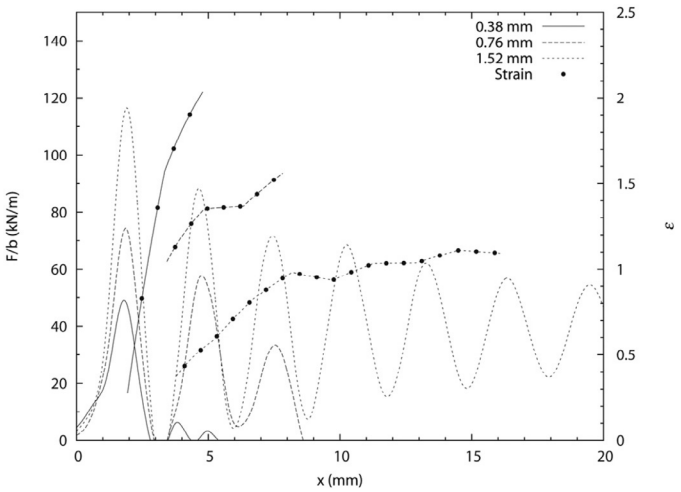

Fig. 15. Experimental force per unit width and strain against the overall deformation for the 10 m/s experiments. The 1.52 mm results are shown up to 20 mm as the exact displacement was difficult to measure after this point due to glass failures; however, force results were collected up to approximately 40 mm displacement for the plateau stress calculation.

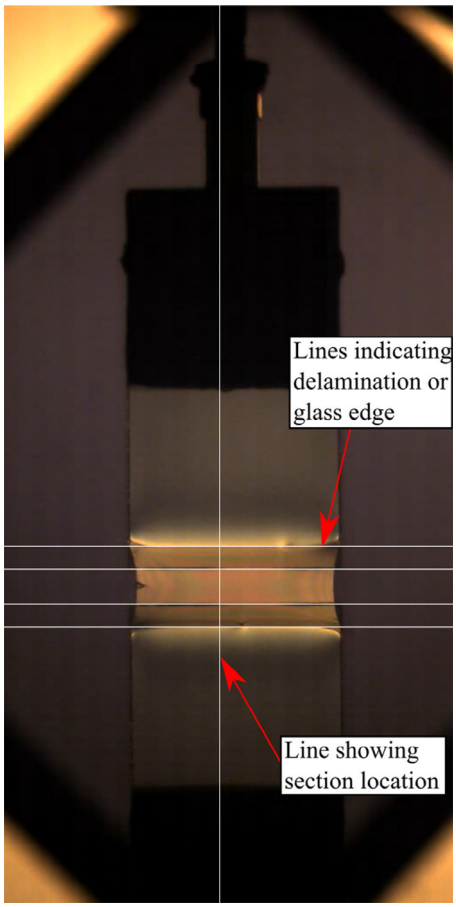

Fig. 16. Experimental test images showing the identified locations of the delamination fronts and glass edges.

Table 7
Experimental delamination speeds for different crack configurations and displacement speed.

Speed Test (m/s)	Delamination speed (m/s)
0.001	0.018 ± 0.001
0.1	0.079 ± 0.004
1	1.40 ± 0.07
10	9.05 ± 0.5

of the bonding layers. However, these data would be required to fit and use more complex delamination models. Instead, a simple logarithmic function was fitted to these data to represent the delamination energy at different nominal rates. The proposed equation was:

$$E_d = a\log(\dot{\varepsilon})^2 + b\log(\dot{\varepsilon}) + c \tag{6}$$

where E_d was the delamination energy expressed in J/m^2, $\dot{\varepsilon}$ was the nominal rate, log represents the base ten logarithm, and a, b and c were fitting constants. The fit was produced using a square minimisation technique and produced the results listed in Table 9. The fitted curve is shown in Fig. 21.

Due to the same difficulties in establishing the deformation rate of the bonding layer, the selection of the peak stress to be used in the model was challenging. For this study, the previously described nominal rate was used. As this was a simple approximation, several models were run varying the peak stresses by 25% above and below the value to be used. In all cases, the plateaux levels did change by a relatively small amount. As an example, the stresses of the 1 m/s model changed by 2.7% when the peak stress was increased by 25%. The effect of this on the estimated energy was calculated, and the possible uncertainty estimated at 7%.

The reduced variability at higher speeds could be used to inform models of the entire window subject to blast loads. Previous blast experiments can be analysed to estimate the range of deformation velocities that would take place during the event. This information could then inform which delamination energy data should be used to simulate the behaviour accurately. This was done by using the DIC data presented by Hooper et al. [8]. A set of data across the centre of the window was considered, and the total length of the line spanning the two window edges was calculated at each time

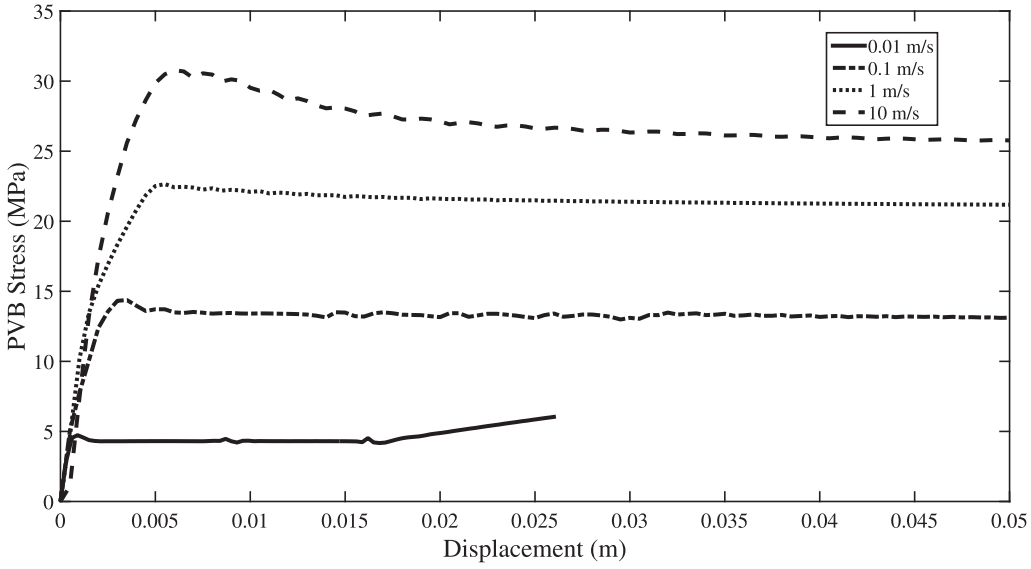

Fig. 17. Single crack delamination model results for 0.1 m/s deformation speed and low rate PVB model.

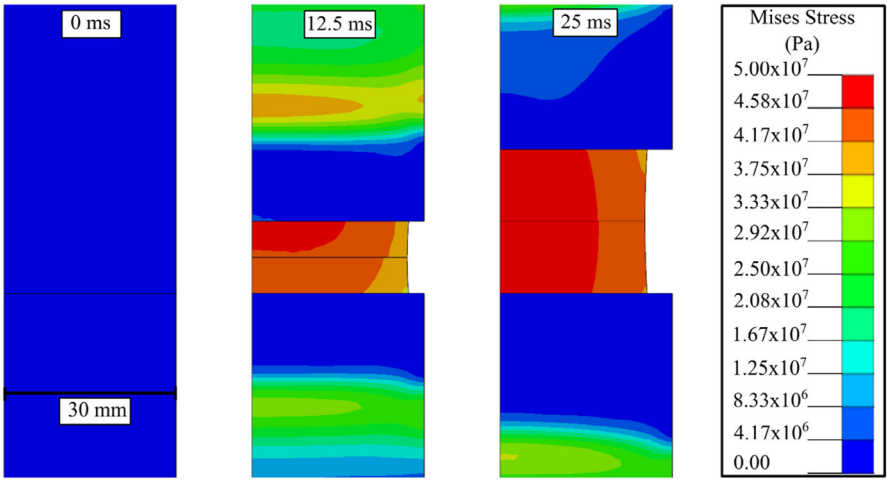

Fig. 18. Progressive delamination of a single crack model deformed at 10 m/s with a low rate PVB model.

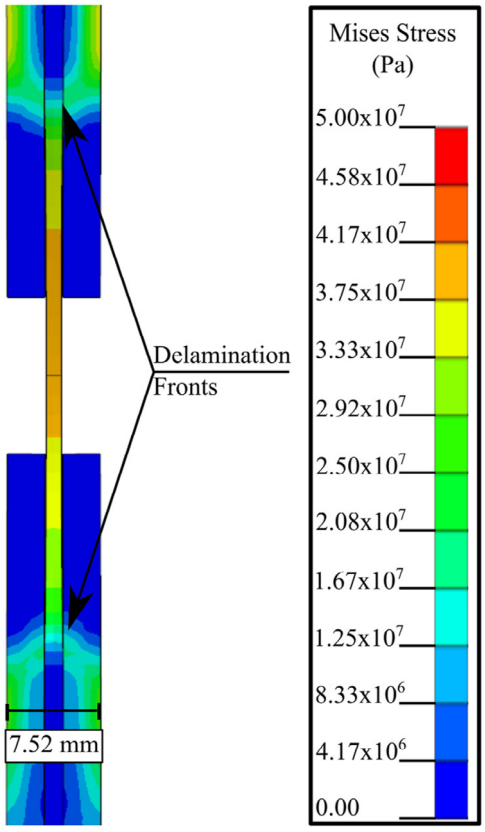

Fig. 19. FEA detail showing the delamination positions.

step from the DIC displacement data. This information was then numerically differentiated to find the deformation speed in one direction and divided by the window length. The results are shown in Fig. 22. The rate of deformation rose between 0.7 and 7.5 s^{-1} before falling rapidly once the maximum deflection was reached, therefore justifying the use of the energy results between these values. These rates, according to the function previously fitted, would produce energies varying between 1725 and 2700 J/m^2. As the most significant delamination would take place after an initial deformation of the cracked glass, it is suspected that an energy of delamination above 2000 J/m^2 would be appropriate for this situation.

As mentioned in the results, the delamination speeds differed slightly from those measured in the experiments. Whilst the disagreement varied between the cases, in general the FEA results showed higher delamination speeds than those measured. This is especially true at lower speeds where the inconsistencies are much higher. It is likely that the discrepancies were caused by the assumptions made in the PVB material model. A stiffer model than seen in reality will increase the delamination speed for a given plateau stress. The delamination progression will require a certain level of force acting across the bonded surface. If the material is stiffer, the membrane strains for this fixed force will be lower. Therefore, more free membrane material will be required to accommodate the overall displacements. The opposite will be the case for a model which is too compliant. The results therefore show that the model employed is generally too stiff. Whilst the overall model used for the fits displayed a lower stiffness at higher strain rates, its stiffness was higher than measured at lower rates, as shown in Fig. 6. The difference in the results is lower for higher deformation speeds, as these would strain the material at higher rates and the PVB would therefore display its higher stiffness due to rate sensitivity. However, even in these cases the used material model is too stiff overall as, further

Table 8
Single crack results.

Deformation speed (m/s)	Deformation rate – Speed/Sample height (s^{-1})	Model plateau stress (MPa)	Energy (J/m^2)	Model delamination speed (m/s)	Experimental delamination speed (m/s)
0.01	0.0667	4.3	90	0.083	0.018
0.1	0.667	13.2	1275	0.245	0.079
1	6.67	21.3	3000	1.87	1.43
10	66.7	26.3	2750	15.67	9.05

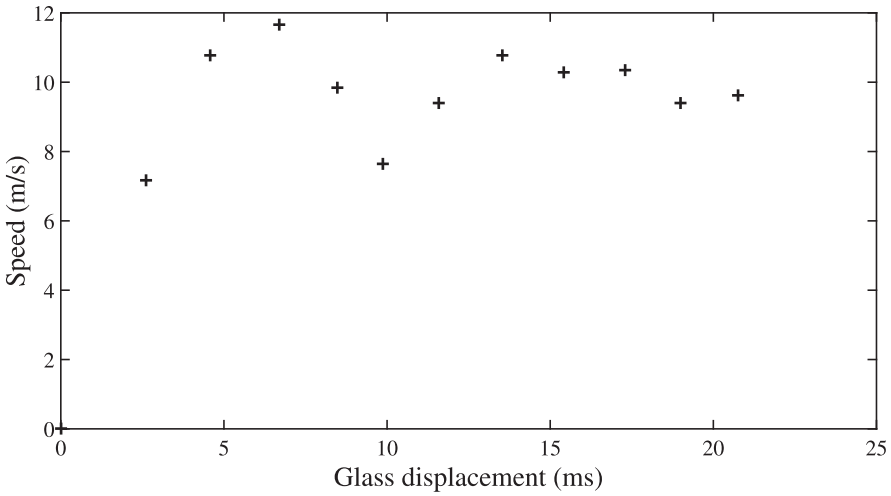

Fig. 20. Glass movement speed in the 10 m/s, 1.52 mm PVB thickness test.

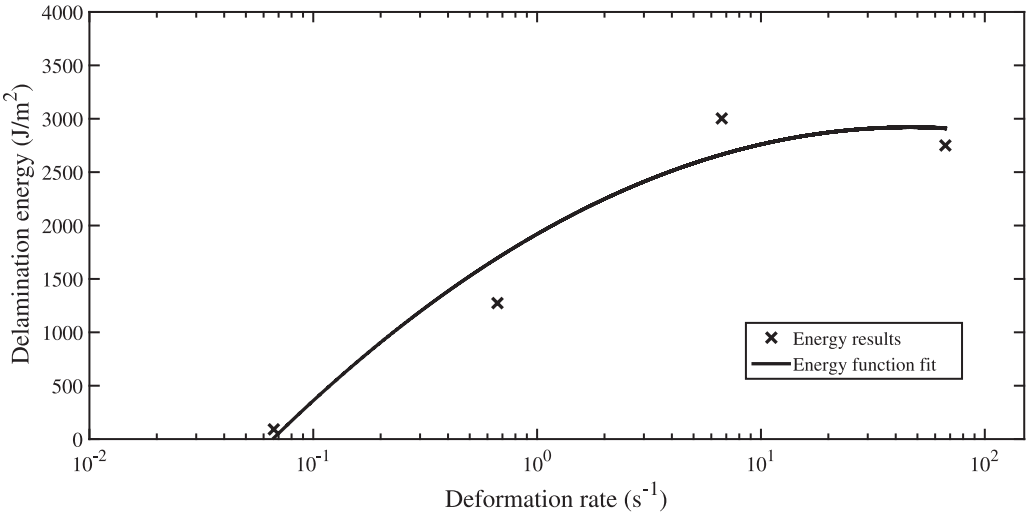

Fig. 21. Delamination energies plotted against the rate of deformation. The deformation energies increase until 6.67 s^{-1}, whilst they seem to be constant after this.

away from the delamination fronts, the deformation rate decreases significantly even in the faster cases. This is shown in Fig. 23, which displays the variation in strain rate in the PVB in the FEA models. The overall PVB strain rate measured from the experimental data also showed significant drops as the ligament lengthened. It should be noted that the rates measured experimentally by differentiating the strains plotted in Figs. 12–15 were different quantities than the FEA ones, as they represented a rate averaged along the whole ligament. Instead, the rates shown in Fig. 23 were instantaneous rates in the specific locations of the PVB. The initial rate values are of the same order of magnitude as the peaks in the figure, as the initial rate found experimentally will be close to the local rate near the delamination fronts in the FEA models. This effect of the PVB material models were highlighted in the case fitted with the low rate model. This showed a significantly reduced delamination speed, as its stiffness was much lower than the main mode fitted. Whilst the speed was much closer to the experimentally measured one, it is suspected that the energy of delamination was not realistic, as it was also dependent on the behaviour of the PVB near the delamination front, where its strain rate was significantly higher. The low stiffness material could not simulate the appropriate behaviour at that stage, as shown in Fig. 7, and it is therefore suggested that the delamination energy produced was not realistic, being mostly valuable as a demonstration of the effect of material models on this parameter. Therefore, these variations of rate across the samples add a significant challenge in representing this phenomenon. The PVB material model ideally would need to represent the entire range of rates, which is challenging using available material models. In this work, the hyperelastic Prony series model does attempt to do this, without,

Table 9
Energy function fit coefficients.

a (J/m^2)	b (J/m^2)	c (J/m^2)
1200	−360	1920

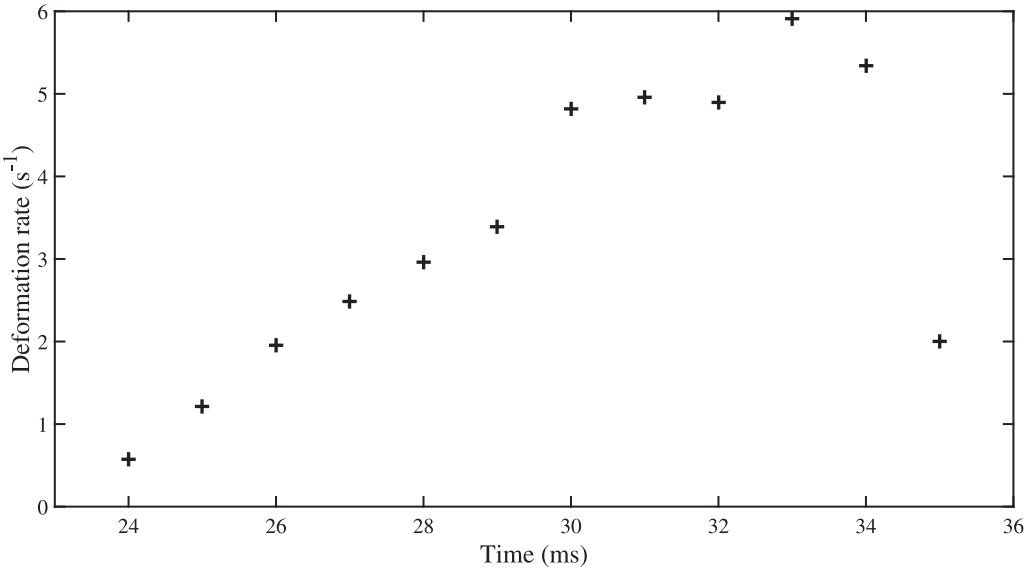

Fig. 22. Nominal rate of deformation during blast loading along a line cut through the centre of the window. The final point shows that the glass was close to its maximum deflection and its expansion speed reduced sharply.

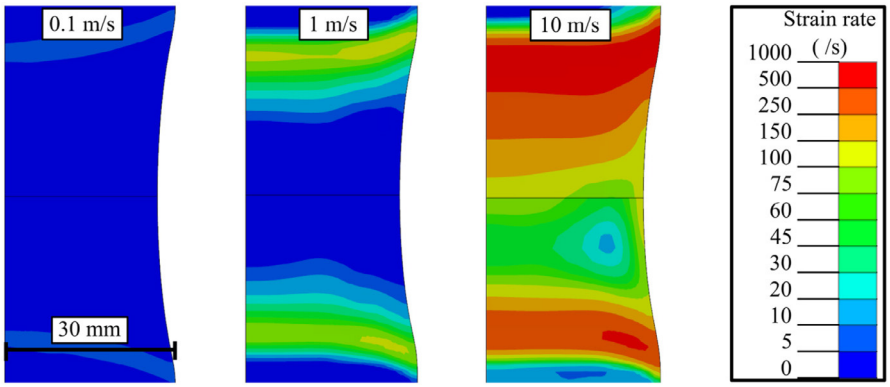

Fig. 23. Image for discussion showing the strain rates developed in the material during the FEA analysis of the tests.

however, being fully able to capture the details of the stress–strain relationships at each speed.

Therefore, whilst the delamination energies presented above will be correct for the specific material model used in their derivation, they might not represent the correct absolute values. It is though suggested that, as the material model produced at least realistic stress estimates at the different strain rates, the energies calculated are likely to be realistic. Further analysis with more refined material models though could improve the estimates. Additionally, should full FEA models of the glazing system be produced including this phenomenon, if the same PVB model suggested here is utilised, the delamination energies suggested would be appropriate to model the debonding process.

5. Conclusion

The delamination of the PVB interlayer from the glass fragments was studied through a series of experiments and FEA models. The experiments were performed on samples with varying interlayer thickness, from 0.38 to 2.28 mm, at different speeds, from 0.01 m/s to 10 m/s. These experiments showed that interlayers thinner than 1.52 mm failed significantly quicker than thicker ones due to the higher levels of strain developed before delamination is initiated. The results also showed that the rate of the PVB deformation changed during the process, decreasing significantly as the delamination front progresses.

A set of the experiments was reproduced using FEA modelling to calculate the delamination energies. The delamination energy was found by fitting the cohesive zone model properties to match the plateau delamination stresses. The 1.52 mm thick interlayer experimental data were employed and the FEA results showed a significant increase in delamination energy for speeds between 0.01 m/s and 0.1 m/s. Delamination energy for speeds of 1 m/s and above was relatively constant. A simple logarithmic function was also fitted to the data to inform the choice of appropriate delamination energies for further modelling works, should a similar material model be adopted. The higher speeds and the more complex PVB material model considered here produced significantly different results when compared with those of previous work, highlighting the importance of these parameters when attempting to quantify this phenomenon.

The additional understanding gained through this research of delamination processes during high rate loading of laminated glass, with different thicknesses of PVB, has been incorporated into design codes for risk analysis of explosive blast threats on glazing elements. This has been done by incorporating these effects into the resistance function in the single degree of freedom system design method which determine important design parameters. This enables more precise designs, improving both the safety and the efficiency of glazing systems.

Acknowledgments

The authors acknowledge Arup Resilience Security and Risk with the Engineering and the Physical Sciences Research Council (EPSRC) for supporting Dr Paolo Del Linz and Dr Paul A. Hooper during their PhDs at Imperial College London and AVIC Beijing Institute of Aeronautical Materials (BIAM), through the AVIC Centre for Material Characterisation, Processing and Modelling, for supporting Dr Yi Wang's and Dr Hari Arora's research on the impact performance of laminated glass windows. The authors also thank the Centre for the Protection of National Infrastructure (CPNI) for providing access to the GL Group test facilities at RAF Spadeadam.

References

[1] Sukhram R. Selection of glazing materials for blast protection In: Glass Processing Days, Finland. 2005.
[2] Zhang X, Hao H, Wang Z. Experimental investigation of monolithic tempered glass fragment characteristics subjected to blast loads. Eng Struct 2014;75:259–75.
[3] Stephens RAC. Determination of the resistance of laminated glass subjected to blast loading using high speed video Master thesis; United Kingdom: Cranfield University. 2008.
[4] Zhang X, Hao H, Wang Z. Experimental study of laminated glass window responses under impulsive and blast loading. Int J Impact Eng 2015;78:1–19.
[5] Zhang X, Hao H. Experimental and numerical study of boundary and anchorage effect on laminated glass windows under blast loading. Eng Struct 2015;90:96–116.
[6] Kranzer C, Gürke G, Mayrhofer C. Testing of bomb resistant glazing systems. Experimental investigation of the time dependent deflection of blast loaded 7.5 mm laminated glass in: Glass Processing Days, Finland, pp. 7. 2005.
[7] Larcher M, Solomos G, Casadei F, Gebbeken N. Experimental and numerical investigations of laminated glass subjected to blast loading. Int J Impact Eng 2012;39:42–50.
[8] Hooper PA, Sukhram RAM, Blackman BRK, Dear JP. On the blast resistance of laminated glass. Int J Solids Struct 2012;49:899–918.
[9] Del Linz P, Hooper PA, Arora H, Smith D, Pascoe L, Cormie D, et al. Reaction forces of laminated glass windows subject to blast loads. Compos Struct 2015;131:193–206.
[10] Keller U., Mortelmans H. Adhesion in Laminated Safety Glass – What makes it work? In Finland, pp. 353–356.
[11] Miller AC, Berg JC. Effect of silane coupling agent adsorbate structure on adhesion performance with a polymeric matrix. Compos Part A Appl Sci Manuf 2003;34:327–32.
[12] Nguyen FN, Berg JC. The effect of vinyl alcohol content on adhesion performance in poly(vinyl butyral)/glass systems. J Adhes Sci Technol 2004;18:1011–26.
[13] Rahul-Kumar P, Jagota A, Bennison SJ, Saigal S. Interfacial failures in a compressive shear strength test of glass/polymer laminates. Int J Solids Struct 2000;37:7281–305.
[14] Muralidhar S, Jagota A, Bennison SJ, Saigal S. Mechanical behaviour in tension of cracked glass bridged by an elastomeric ligament. Acta Mater 2000;48:4577–88.
[15] Butchart C, Overend M. Delamination in fractured laminated glass in: Engineered transparency. International Conference at glasstec, Dusseldorf, Germany. 2012.

[16] Iwasaki R, Sato C, Latailladeand JL, Viot P. Experimental study on the interface fracture toughness of PVB (polyvinyl butyral)/glass at high strain rates. Int J Crashworth 2007;12:293–8.
[17] Pelfrene J, Van Dam S, Van Paepegem W. Numerical analysis of the peel test for characterisation of interfacial debonding in laminated glass. Int J Adhes Adhes 2015;62:146–53.
[18] Vallabhan C, Das Y, Ramasamudra M. Properties of PVB Interlayer Used in Laminated Glass. J Mater Civ Eng 1992;4:71–6.
[19] Du Bois PA, Kolling S, Fassnacht W. Modelling of safety glass for crash simulation. Comput Mater Sci 2003;28:675–83.
[20] Timmel M, Kolling S, Osterrieder P, Du Bois PA. A finite element model for impact simulation with laminated glass. Int J Impact Eng 2007;34:1465–78.
[21] Xu J, Li Y. Crack analysis in PVB laminated windshield impacted by pedestrian head in traffic accident. Int J Crashworth 2009;14:63–71.
[22] Xu J, Li Y, Ge D, Liu B, Zhu M. Experimental investigation on constitutive behavior of PVB under impact loading. Int J Impact Eng 2011;38:106–14.
[23] Iwasaki R, Sato C. The influence of strain rate on the interfacial fracture toughness between PVB and laminated glass. J Phys IV France 2006;134:1153–8.
[24] Morison C. The resistance of laminated glass to blast pressure loading and the coefficients for single degree of freedom analysis of laminated glass thesis. 2007.
[25] Hooper PA, Blackman BRK, Dear JP. The mechanical behaviour of poly(vinyl butyral) at different strain magnitudes and strain rates. J Mater Sci 2012;47:3564–76.
[26] Liu B, Sun Y, Li Y, Wang Y, Ge D, Xu J. Systematic experimental study on mechanical behavior of PVB (polyvinyl butyral) material under various loading conditions. Polym Eng Sci 2012;52:1137–47.
[27] Zhang X, Hao H, Shi Y, Cui J. The mechanical properties of polyvinyl butyral (PVB) at high strain rates. Constr Build Mater 2015;93:404–15.
[28] Goh SM, Charalambides MN, Williams JG. Determination of the constitutive constants of non-linear viscoelastic materials. Mech Time-Depend Mater 2004;8:255–68.
[29] Dassault Systèmes Simulia Corp.. Abaqus analysis manual v6.9 Providence, RI. 2009.
[30] Chandra N, Li H, Shet C, Ghonem H. Some issues in the application of cohesive zone models for metal–ceramic interfaces. Int J Solids Struct 2002;39:2827–55.
[31] Hooper P. Blast performance of silicone-bonded laminated glass Ph.D. thesis; United Kingdom: Imperial College London. 2011.
[32] Zhang X, Shi Y, Hao H, Cui J. The mechanical properties of ionoplast interlayer material at high strain rates. Mater Des 2015;83:387–99.
[33] Marzi S, Hesebeck O, Brede M, Kleiner F. A rate-dependent cohesive zone model for adhesively bonded joints loaded in mode I. pp. 881–898; 2009.
[34] Hallquist JO. LS-DYNA keyword user's manual V. 970 Livermore Software Technology Corp.. 2007.